



CrossMark  
 click for updates

Cite this: *RSC Adv.*, 2015, 5, 5754

## Electrostatically-induced trajectory switching system on a multi-inlet-multi-outlet superhydrophobic droplet guiding track†

Soonil Lee, ‡<sup>a</sup> Seulah Lee, ‡<sup>a</sup> Dayeong Kim,<sup>a</sup> Jungmok Seo,<sup>a</sup> Chandreswar Mahata,<sup>a</sup> Hyunseok Hwang,<sup>b</sup> Hassan Algadi,<sup>ac</sup> Saleh Al-Sayari,<sup>c</sup> Youngcheol Chae<sup>b</sup> and Taeyoon Lee<sup>\*a</sup>

A multi-inlet-multi-outlet (MIMO) superhydrophobic droplet guiding track was demonstrated for water droplet manipulation using an electrostatic force-induced trajectory switching system. Without applying an external electrostatic field, the water droplet rolled along the superhydrophobic guiding track due to its extreme water repellent properties and gravitational force. By applying a DC bias to a capacitor above the guiding track, the trajectory of the water droplet can be easily controlled by the electrostatic attraction. Electrostatically-induced trajectory switching was successfully achieved when the electrostatic and gravitational forces exerted on the water droplet were properly balanced. On a MIMO superhydrophobic droplet guiding track with three inlets and four outlets, the water droplet was guided along the intended trajectory.

Received 23rd October 2014  
 Accepted 8th December 2014

DOI: 10.1039/c4ra13014f

[www.rsc.org/advances](http://www.rsc.org/advances)

### Introduction

Open channel microfluidic systems have been widely researched due to their considerable advantages in terms of cost, accessibility, and simplicity. These systems can be applied to various fields, including in micro reactors,<sup>1–4</sup> water harvesting,<sup>5,6</sup> and solution transfer.<sup>7–11</sup> In particular, open channel microfluidic systems allow functional laboratory operations (e.g., chemical reactions, transportation) to be performed rapidly and efficiently with small-volume droplets. Conventionally, gravitational force has been used in combination with hydrophilic-patterned superhydrophobic surfaces to guide and transport water droplets. Mussel-inspired polydopamine micropatterning on superhydrophobic anodized aluminum oxide,<sup>3</sup> hydrophilic patterned superhydrophobic Si nanowire arrays,<sup>8</sup> high surface energy ink printing on superhydrophobic paper,<sup>4,12,13</sup> and TiO<sub>2</sub> nanostructures with hydrophilic micropatterning by photocatalytic lithography<sup>14</sup> are examples of this technology. However, patterned hydrophilic microfluidic channels cause contamination of the guiding tracks and loss of

water during the transportation. Recently, Mertaniemi *et al.* reported a water droplet guiding system using a mechanically grooved superhydrophobic copper (Cu) substrate.<sup>9</sup> On this substrate, water droplets can roll along the grooved guiding track without losing water or contaminating the surface due to the water-repellent properties of the superhydrophobic substrate.

Among the various systems of water droplet manipulation, electric force has been used frequently due to its short response time and facile operation. Several studies on the manipulation of water droplets have been reported using electrostatic charged capacitors,<sup>15</sup> directional electric fields generated by parallel-strip electrodes,<sup>16</sup> or electrically-tunable wetting defects on superhydrophobic surfaces.<sup>17</sup> Using these methods, it is possible to manipulate water droplets minutely for transportation,<sup>18</sup> sorting,<sup>19</sup> merging,<sup>20,21</sup> and splitting.<sup>22</sup> However, water droplets are exposed to the electrostatic field during the manipulation process, and should be continuously in contact with electrodes. Kawamoto *et al.* reported the use of electrostatic probes with dipole electrodes to manipulate a small single particle using instantaneously applied high voltage.<sup>23</sup> Small single particles can be manipulated utilizing electrostatic probes instantaneously applied with high voltage without any mechanical contact between particles and probes. This manipulation method using electrostatic force could be advantageous for water droplet manipulation, since unnecessary mechanical contact and continuous exposure to the electrostatic field which could induce the undesired effects on the water droplet can be avoided.

<sup>a</sup>Nanobio Device Laboratory, School of Electrical and Electronic Engineering, Yonsei University, 50 Yonsei-ro, Seodaemun-Gu, Seoul 120-749, Republic of Korea. E-mail: taeyoon.lee@yonsei.ac.kr

<sup>b</sup>Mixed Signal IC Laboratory, School of Electrical and Electronic Engineering, Yonsei University, 50 Yonsei-ro, Seodaemun-Gu, Seoul 120-749, Republic of Korea

<sup>c</sup>Promising Center for Sensors and Electronic Devices (PCSED), Najran University, P.O. Box 1988, Najran 11001, Saudi Arabia

† Electronic supplementary information (ESI) available. See DOI: 10.1039/c4ra13014f

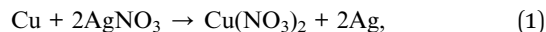
‡ These authors equally contributed to this work.

In this work, we demonstrated an electrostatic-induced trajectory switching system on a high-speed multi-inlet-multi-outlet (MIMO) superhydrophobic droplet guiding track without any mechanical contact. Droplet guiding tracks were fabricated by sculpturing a shadow groove structure on a Cu plate using a computer numerical control (CNC) milling method. In order to obtain the superhydrophobic surface, Ag nanostructures were formed on the groove-structured Cu plate using electroless galvanic deposition, followed by dip-coating in 1*H*,1*H*,2*H*,2*H*-perfluorodecanethiol (PFDT). Water droplets rolled off the surface along the grooved guiding track with negligible frictional force, leaving the surface free of contaminants. Two identical capacitors, patterned back-to-back on a glass, were located above the junction of the 'reversed Y-shaped' groove structure on the Cu plate in order to exert electrostatic force. The electrostatic force was generated by applying a 1 kV DC bias to the capacitor. By alternatively applying the active electrostatic-induced capacitors, the trajectory of a moving water droplet could be controlled. The electrostatic-induced trajectory switching system was successfully applied to the MIMO open channel microfluidic system, which has three inlets and four outlets.

## Materials and methods

### Fabrication of PFDT Ag/Cu guiding track

The PFDT Ag/Cu guiding track was fabricated on a 1 mm-thick Cu plate. The starting substrate was a sculptured Cu plate with shadow grooves which had a width of 1.5 mm and a depth of 0.5 mm using a CNC mechanical milling method.<sup>9</sup> On the sculptured Cu plate, Ag dendrites were grown by a galvanic deposition process.<sup>24</sup> The sculptured Cu plate was cleaned with a solution mixture of NH<sub>4</sub>OH–H<sub>2</sub>O<sub>2</sub>–H<sub>2</sub>O (volume ratio of 1 : 1 : 5) at 60 °C for 10 min to remove surface organic contaminants. The copper oxide on the Cu surface was removed by dipping it into a 20% CH<sub>3</sub>COOH aqueous solution for 1 h at 40 °C. After cleaning the substrates, they were immersed into an aqueous solution of 3 mM AgNO<sub>3</sub> at 30 °C for 30 min. Ag<sup>+</sup> ions that were dissolved in the aqueous solution and chemically reacted with Cu atoms. Due to the difference in their ionization tendencies, Ag<sup>+</sup> ions changed to Ag atoms when Cu atoms were converted into Cu<sup>2+</sup> ions as follows:



Reacted Ag atoms grew with a double-roughness structure on the Cu surface. Then, the chemical superhydrophobic coating process was carried out by immersing the substrate in a 1 mM solution of PFDT dissolved in ethanol for 1 h at room temperature. After coating PFDT on the substrates, they were rinsed with ethanol to remove any residual organic reactants. The substrates were baked at 70 °C for 30 min to obtain a uniform PFDT layer.

### Capacitor circuit patterning on the glass slide

To exert electrostatic force on the water droplet, a capacitor circuit was patterned on a glass slide. A 50 nm-thick Ti layer and

a 300 nm-thick Cu layer were subsequently deposited on the glass slide with a patterned shadow mask using a thermal evaporator. As shown in Fig. S1,<sup>†</sup> the circuit pattern consists of capacitors, electrodes, and connectors. The as-prepared PFDT Ag/Cu guiding track was located beneath the circuit-patterned glass slide at a spacing distance of 2 mm. Two capacitors of the patterned circuit were located above the left and right sides of the junction region.

### Exerting electrostatic force

The as-fabricated circuit-patterned glass slide was connected with a high voltage power supply (PS325, Stanford Research Systems) to apply the DC power source. When a capacitor of the patterned circuit was biased by the DC power source with a 1 kV, strong electrostatic fields could be generated near the capacitor.

### Characterization

The surface morphologies of the Ag dendrite-covered Cu plate were observed using a JEOL JSM-7001F field emission scanning electron microscope (FE-SEM). Water contact angles (CAs) were measured by a dynamic image capture camera (DSC-T30, SONY Co., Ltd.). The numerical simulation results were performed using a commercial numerical solver (COMSOL Multiphysics 4.3).

## Results and discussions

In order to obtain a superhydrophobic surface for the droplet guiding track, a PFDT Ag/Cu plate was fabricated. The Ag layer of the PFDT Ag/Cu plate was formed by the growth of nanostructures using the electroless galvanic deposition method.<sup>24</sup> The surface morphologies of the nanostructured Ag layer were changed depending on the galvanic reaction time. To observe the change in the surface wetting properties of the PFDT Ag/Cu plate, static water contact angles (CAs) and water sliding angles (SAs) were observed at different electroless galvanic deposition times. Fig. 1a shows the CAs and SAs of water droplets on the surface of the PFDT Ag/Cu plate as a function of galvanic reaction time. On the flat Cu plate coated with PFDT, the water CA was 117.3° and the water SA was greater than 90°. The water CAs moderately increased and saturated at CAs ≥ 160° when the reaction times were higher than 20 min. On the other hand, the water SA drastically decreased in between reaction times of 1 min and 5 min, followed by a gradual decrease and saturation of the SA ≈ 1°. Fig. 1b shows typical top-view FE-SEM micrograph illustrating the morphology of the PFDT Ag/Cu surface with galvanic reaction for 30 minutes. Ag nanostructures were found randomly distributed over a large area and formed a double-roughness structure on the Cu plate. The Ag nanostructures were composed of a combination of clusters (ranging in size from 300 nm to 1 μm) and small Ag particles (ranging between 100 nm and 200 nm) on the Cu surface. This double-roughness structure is known to be a favorable structure for the formation of a superhydrophobic surface.<sup>25</sup> In order to convert the Ag/Cu plate to a superhydrophobic surface, the substrate was also coated with PFDT, which has low surface tension (14.8 mN m<sup>-1</sup>).

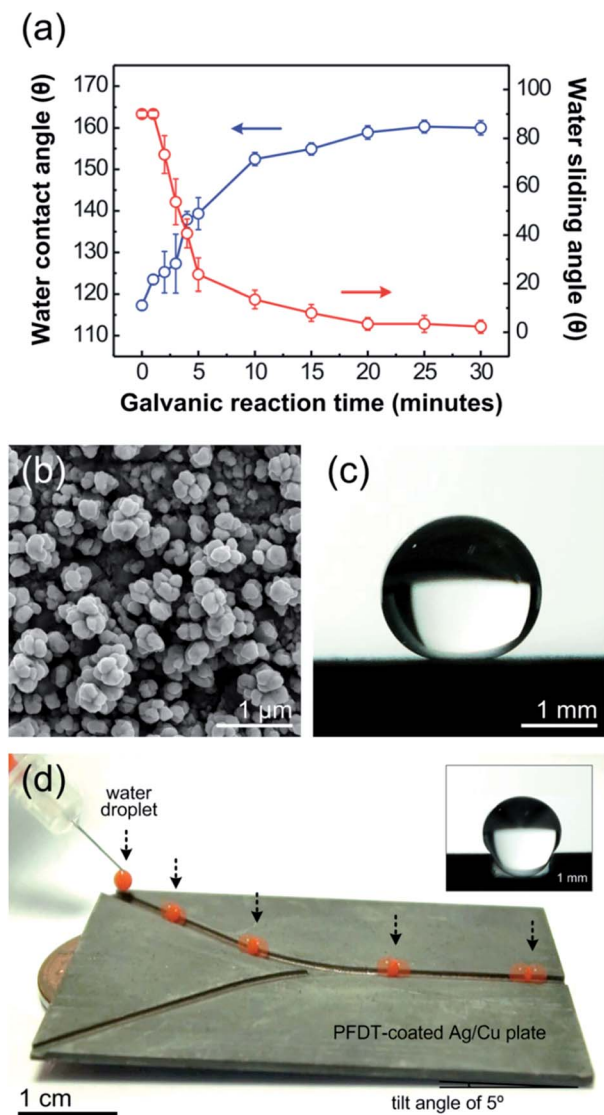


Fig. 1 (a) Water CAs (blue symbol along left axis) and SAs (red symbol along right axis) of 5  $\mu\text{L}$  droplets on the surface of the PFDT Ag/Cu plate as a function of galvanic reaction time. (b) Typical SEM image of the top view of the PFDT Ag/Cu surface, and (c) an optical image of a 5  $\mu\text{L}$  water droplet on the PFDT Ag/Cu plate (at a galvanic reaction time of 30 min). (d) Sequential photographic images of a moving water droplet (5  $\mu\text{L}$ ) along the PFDT Ag/Cu guiding track (the inset shows the optical image of a water droplet on the groove-structured guiding track).

Fig. 1c is a photograph of a static water droplet on the flat surface of the PFDT Ag/Cu plate at 30 min of galvanic reaction time. The water droplet has a high CA of  $160 \pm 1.23^\circ$  on the flat surface of the PFDT Ag/Cu plate. The PFDT Ag/Cu plate demonstrated extreme water-repellent properties.

Fig. 1d shows a sequence of images of a 5  $\mu\text{L}$  water droplet moving along the 'Y-shaped' PFDT Ag/Cu guiding track. In the photographs, the locations of the water droplet are marked with black dotted arrows. Due to the highly water repellent property of the PFDT Ag/Cu surface, the water droplet successfully rolled off the surface along the curved PFDT Ag/Cu guiding track at a

low tilt angle of  $5^\circ$ . The measured velocity of the moving water droplet on the PFDT Ag/Cu guiding track was  $5.71 \text{ cm s}^{-1}$  under the given tilt angle. As shown in the inset of Fig. 1d, the shape of the water droplet along the PFDT Ag/Cu guiding track was deformed to adapt to the groove structure due to gravitational and surface tension forces. The groove structure in our experiment helped the water droplet move along the guiding track as well as partially supporting the weight of the droplet by the bottom of the groove structure. The degree of deformation of water droplets induced by the edge of the groove structure affects the maximum velocity ( $v_m$ ) at which the water droplet is successfully guided along the curve of the guiding track.<sup>9</sup> When the degree of deformation of water droplets as a result of gravitational force on the groove structure is increased,  $v_m$  is decreased. Lower  $v_m$  indicates that the droplets can be easily misguided. Thus, we use the groove structure with bottom to minimize the  $v_m$  lowering effect from deformed droplet by gravitational force.

To investigate the electrostatically-induced trajectory switching system using the PFDT Ag/Cu guiding track, the systematic movements of water droplets on the guiding track were observed by alternatively applying 1 kV voltage to the capacitors patterned on the glass slide. Fig. 2a is a schematic illustration of the experimental set up of the electrostatically-induced trajectory switching system. The 'reversed Y-shaped' PFDT Ag/Cu guiding track was kept with a low tilt angle of  $5^\circ$  and electrically grounded. The substrate was located under the capacitor-patterned glass slide at a distance of 2 mm. The junction part of the PFDT Ag/Cu guiding track is emphasized with a black dotted square. The inset of Fig. 2a shows the details of the black dotted-square region. The PFDT Ag/Cu guiding track was divided into two different tracks, which were bisymmetrical at the junction. On the bottom of the glass slide, anodes and cathodes of capacitors were patterned *via* four 1 mm-diameter circles.

Fig. 2b and c show time sequence images of moving water droplets (5  $\mu\text{L}$ ) on the 'reversed Y-shaped' PFDT Ag/Cu guiding track located under the circuit-patterned glass slide and the Video S1.† The droplets were moved depending on the direction of the 1 kV DC bias applied using the left-side or right-side capacitors. In these images, the locations of the moving water droplet are indicated by black dotted arrows. The anode and cathode electrodes of the patterned capacitor at 1 kV DC bias are colored with red and blue, respectively. When a water droplet was dropped from a micro-needle, it was rolled-off along the PFDT Ag/Cu guiding track until it reached the junction part of the guiding track. At the junction, an electrostatic force was exerted on the water droplet by the DC-biased capacitor. When high voltage was applied to the patterned capacitors, charges were accumulated at the edges of both anode and cathode electrodes. Due to the accumulation of charges, the strong electrostatic fields could be generated near the capacitor. Then, as the water droplet passed through the junction, it was attracted toward the DC-biased capacitor due to the electrostatic force. The trajectory of the moving water droplet was successfully changed by alternately generating electrostatic force; the direction of the droplet trajectory was switched by the position

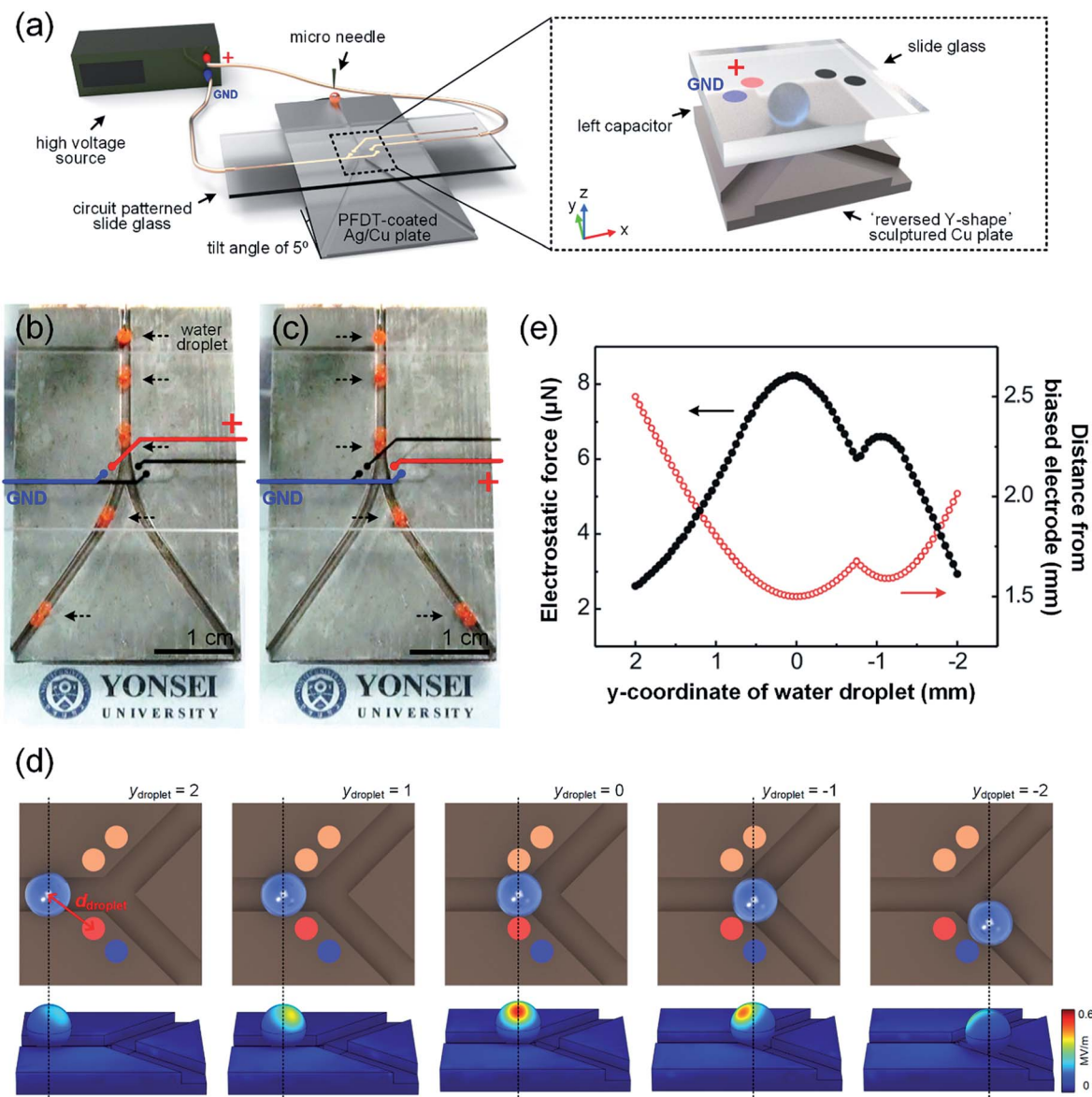


Fig. 2 Schematic illustration of (a) experimental set up for the electrostatic-induced trajectory switching system and simulation model at the junction part of the PFDT Ag/Cu guiding track. Sequential photographic images of a moving water droplet (5  $\mu$ L) on the 'reversed Y-shaped' PFDT Ag/Cu guiding track located under the circuit-patterned glass slide when (b) the left-side and (c) the right-side capacitors of the patterned circuit were applied with 1 kV DC bias, respectively (see the Video S1†). (d) Electrostatic field distributions on the surface of water droplets at different locations on the PFDT Ag/Cu guiding track. (e) Calculated electrostatic force exerted on the water droplet (black symbol along left axis) and  $d_{\text{droplet}}$  (red symbol along right axis) with respect to  $y_{\text{droplet}}$  between 2 mm and  $-2$  mm in the simulation model.

of the DC-biased capacitor. Furthermore, we also tried to control the canola oil droplet to verify the effects of electrostatic force on other liquids, however, the electrostatic attraction for sufficient water guiding was not generated. The reason could be attributed to the non-polar characteristic of the canola oil droplet. Since the polarized surface charge of the canola oil droplet by applied electrostatic field would not be generated, the electrostatic force cannot be occurred.

When the water droplet passed through the junction of the 'reversed Y-shape' PFDT Ag/Cu guiding track, the dynamics of electrostatic field distributions on the surface of the water droplet were analyzed using the commercial numerical solver,

COMSOL Multiphysics 4.3, based on the electrostatic module. The simulation model of the junction of the 'reversed Y-shape' PFDT Ag/Cu guiding track was structured as seen in the inset of Fig. 2a. In this simulation, the bottom substrate and the blue-colored cathode of the capacitor were electrically grounded and the red-colored anode of the capacitor was biased with a 1 kV DC source. We assume that the water droplet on the guiding track could be approximate by a 1 mm-radius sphere. Although the shape of the water droplet was changed slightly by the groove structure of the guiding track, water droplet deformation was minimized by the support of the bottom of the track as shown in Fig. 1d. Electrowetting, which occurred as a result of

the electrostatic field on the surface of the substrate, could be happened. However, the water droplet was mainly affected by electrostatic fields when it passed the junction region along the guiding track. Because of the rapid speed of the water droplet ( $5.71 \text{ cm s}^{-1}$ ), this junction region was passed within  $0.08 \text{ s}$ . Furthermore, the electrostatic field on the surface of the substrate is relatively low ( $\sim 0.1 \text{ MV m}^{-1}$ ).<sup>15</sup> Thus, the shape change of water droplet by electrowetting in this region was negligible. The physical parameters used in the simulation are presented in Table 1. Fig. 2d represents the sequential electrostatic field distributions on the surface of the water droplet as it moved along the guiding track. The location of the water droplet on the guiding track in the simulation model was varied by decreasing the  $y$ -coordinate of the water droplet ( $y_{\text{droplet}}$ ) from  $2 \text{ mm}$  to  $-2 \text{ mm}$ . At each position, the electrostatic field on the surface of the water droplet was concentrated toward the direction of the DC-biased capacitor; however, the strength of the electrostatic fields was different at each location. When the water droplet was located at  $y_{\text{droplet}} = 2 \text{ mm}$ , it was negligibly affected by the electrostatic fields. At  $y_{\text{droplet}} = 1 \text{ mm}$ , weak electrostatic fields were generated near the upper surface of the water droplet. Between  $y_{\text{droplet}} = 2 \text{ mm}$  and  $0 \text{ mm}$ , the electrostatic fields on the surface of the water droplet became strong because the distance between the water droplet and the anode of the DC-biased capacitor ( $d_{\text{droplet}}$ ) was decreased. At  $y_{\text{droplet}} = 0 \text{ mm}$ ,  $d_{\text{droplet}}$  was smallest; the electrostatic fields on the surface of the water droplet were strongest, reaching a maximum value of  $0.59 \text{ MV m}^{-1}$ . A  $y_{\text{droplet}}$  value of less than  $0 \text{ mm}$  suggested that electrostatic fields were weakening on the surface of the water droplet. At  $y_{\text{droplet}} = -2 \text{ mm}$ , the electrostatic fields on the surface of the water droplet were negligible.

The water droplet was attracted toward the DC-biased capacitor by electrostatic forces due to the concentrated electrostatic fields on the surface of the water droplet. The electrostatic force exerted on a water droplet ( $\vec{F}_e$ ) can be calculated using the Maxwell stress tensor method.<sup>26</sup> When charges were accumulated on the surface of the water droplet, electrostatic fields were exerted onto the water droplet without inducing any electrostatic fields inside the droplet. Therefore, according to the Maxwell stress tensor  $f$ ,  $\vec{F}_e$  can be calculated using the numerical solver as follows:

$$\vec{F}_e = \int_S f dS, \quad (2)$$

$$f = \frac{1}{2} \epsilon_0 \epsilon_r (\vec{E})^2, \quad (3)$$

where  $S$  is the surface area of the water droplet,  $\epsilon_0$  is the permittivity of free space,  $\epsilon_r$  is the relative permittivity of the water droplet and  $\vec{E}$  is the electrostatic field.  $\vec{E}$  is determined by

the Coulomb's law and the superposition principle as shown in eqn (4).

$$\vec{E} = \frac{1}{4\pi\epsilon_0} \sum_{i=1}^N \left( \frac{Q_i}{r_i^2} \vec{r}_i \right), \quad (4)$$

where  $N$  is the number of point charges,  $Q_i$  is the electric charge of the  $i$ -th point charge, and  $\vec{r}_i$  is the corresponding unit vector of  $r_i$  which is the position of charge  $Q_i$  with respect to the point of interest. The boundary conditions are as follows:

$$\vec{E} = -\nabla\phi, \text{ where } \phi \text{ is the potential} \quad (5)$$

$$\phi = 1 \text{ kV, (anode electrode)}$$

$$\phi = 0, \text{ (cathode electrode)}$$

According to these equations,  $\vec{F}_e$  was proportional to the square of  $\vec{E}$  and  $\vec{E}$  was inversely proportional to the square of the distance between charges and the surface of water droplets. In other words, higher electrostatic force indicates a stronger electrostatic field, which could occur with decreased distance between the water droplet and the anode of the DC-biased capacitor. Fig. 2e shows the relationship between  $d_{\text{droplet}}$  (red symbol) and the calculated electrostatic force exerted on the water droplet (black symbol) as  $y_{\text{droplet}}$  is varied from  $2 \text{ mm}$  to  $-2 \text{ mm}$ . While the water droplet moves from the position of  $y_{\text{droplet}} = 2 \text{ mm}$  to  $y_{\text{droplet}} = 0 \text{ mm}$ , the electrostatic force sharply increased with decreasing  $d_{\text{droplet}}$  towards the electrostatic-induced capacitor. The electrostatic force was strongest at  $y_{\text{droplet}} = 0 \text{ mm}$  ( $8.21 \mu\text{N}$ ) due to the smallest  $d_{\text{droplet}}$ . From  $y_{\text{droplet}} = 0 \text{ mm}$  to  $y_{\text{droplet}} = -0.75 \text{ mm}$ , the electrostatic force on the water droplet decreased as a result of increasing  $d_{\text{droplet}}$ . In this region, the trajectory of the water droplet could be influenced by the direction of the electrostatic force induced by the DC-biased capacitor. After the water droplet was guided toward the DC-based capacitor, it was closer to the anode of the DC-biased capacitor at  $y_{\text{droplet}} = -1 \text{ mm}$ . The electrostatic force on the water droplet increased slightly again between  $y_{\text{droplet}} = -0.75 \text{ mm}$  and  $y_{\text{droplet}} = -1 \text{ mm}$  because  $d_{\text{droplet}}$  had decreased slightly. When the water droplet passed  $y_{\text{droplet}} = -1 \text{ mm}$ , the electrostatic force decreased due to the increase in  $d_{\text{droplet}}$  again. These simulation results indicate that the electrostatic force exerted on the water droplet has a strong inversely proportional relationship with  $d_{\text{droplet}}$ .

To investigate the effects of DC-biased capacitors on the water droplet, the electrostatic force exerted on the water droplet was analyzed by varying the applied voltage and measuring the trajectory of the moving water droplet. When the water droplet was at the junction part of the 'reversed Y-shaped' PFDT Ag/Cu guiding track, the force exerted on the water droplet could be divided by two perpendicular forces on the horizontal plane: the  $x$ -directional electrostatic force ( $F_{ex}$ ) and the  $y$ -directional gravitational force ( $F_g$ ). The  $F_g$  can be expressed by  $mg \sin \theta_{SA}$ , where  $m$  is the mass of water droplet,  $g$  is the

Table 1 Physical properties

Conductivity of Cu	$5.998 \times 10^7 \text{ S m}^{-1}$
Relative dielectric constant of liquid water	78
Relative dielectric constant of glass	4.2
Relative dielectric constant of air	1

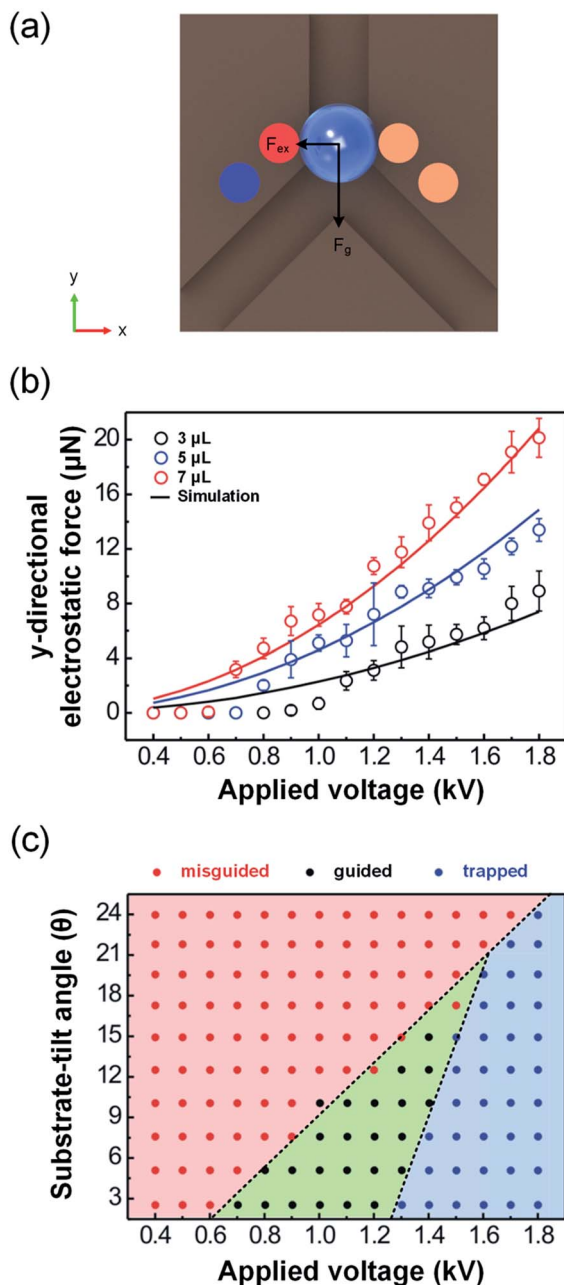


Fig. 3 (a) Schematic illustration of the  $F_{ex}$  and  $F_g$  that affected a water droplet at the junction part of the 'reversed Y-shaped' PFDT Ag/Cu guiding track. (b) The experimental- $F_{ex}$  and simulated- $F_{ex}$  of water droplets of 3  $\mu\text{L}$ , 5  $\mu\text{L}$ , and 7  $\mu\text{L}$  as a function of applied voltage. (c) Red, black, and blue symbols indicate 'misguided', 'guided', and 'trapped', respectively, as a function of substrate-tilt angle and applied voltage. (Red-shaded region: 'misguided', green-shaded region: 'guided', and blue-shaded region: 'trapped'.)

gravitational acceleration constant, and  $\theta_{SA}$  is water sliding angle. Fig. 3a shows a schematic illustration of the  $F_{ex}$  and  $F_g$  exerted on the moving water droplet at the junction. In our experiment, since the PFDT Ag/Cu guiding track was maintained with a constant low tilt angle of  $5^\circ$ , the  $F_g$  was constant. On the other hand, the  $F_{ex}$  was significantly altered according to the applied voltage. The  $F_{ex}$  could be estimated by observing  $\theta_{SA}$ ,

which is the critical tilt angle when the water droplet was rolled-off along the substrate.<sup>27,28</sup> In order to estimate the  $F_{ex}$ , a measurement system was manufactured using a line-patterned PFDT Ag/Cu guiding track and a single capacitor-patterned glass slide, as shown in the Fig. S2.† In our measurement system, there are two forces that mainly affect the movement of the water droplet: the gravitational force of the water droplet at a certain sliding angle ( $F_{SA}$ ) and the  $F_{ex}$  caused by the DC-biased capacitor. When the substrate was tilted at the  $\theta_{SA}$ , the  $F_{SA}$  becomes equivalent to the  $F_{ex}$ . In this case, the relationship between the  $F_{ex}$  and  $\theta_{SA}$  can be expressed as follows:

$$F_{ex} = -\rho Vg \sin \theta_{SA}, \quad (6)$$

where  $\rho$  is the water density, and  $V$  is the droplet volume. At first, the  $\theta_{SA}$  of a 5  $\mu\text{L}$  water droplet was determined with the measurement system when the DC bias voltage applied to the capacitor was varied from 0.4 kV to 1.8 kV. According to eqn (6), the  $F_{ex}$  was estimated using the measured  $\theta_{SA}$ ,  $1 \text{ g cm}^{-3}$  for the water density, and  $9.8 \text{ m s}^{-2}$  as  $g$ . In addition, the  $F_{ex}$ , which was experimentally estimated with the measured  $\theta_{SA}$  (experimental- $F_{ex}$ ), was compared with the simulation result of the  $F_{ex}$  calculated by the numerical solver (simulated- $F_{ex}$ ). Fig. 3b represents the variations of the experimental- $F_{ex}$  fitted with the simulated- $F_{ex}$  with respect to the applied voltage. The results show that when the applied voltage was below 0.7 kV, the water droplet rolled-off at a  $\theta_{SA}$  of  $\sim 0^\circ$ . In this case, the experimental- $F_{ex}$  could not be estimated since sufficient electrostatic force to control the water droplet was not applied. When the applied voltage was increased, both the experimental- $F_{ex}$  and simulated- $F_{ex}$  were substantially increased. The experimental- $F_{ex}$  was fitted to the simulated- $F_{ex}$  within a relative error of 10.1%. Furthermore, in order to investigate the aspect of electrostatic-induced trajectory switching system with various volumes of water droplets, the experimental- $F_{ex}$  and simulated- $F_{ex}$  were also observed at different volumes of water droplets (3  $\mu\text{L}$  and 7  $\mu\text{L}$ ). Despite the difference in volume, the measured  $\theta_{SA}$  of 3  $\mu\text{L}$  and 7  $\mu\text{L}$  water droplets were similar with the  $\theta_{SA}$  of 5  $\mu\text{L}$  water droplets (Fig. 3b). It could be attributed that when the  $F_{SA}$  changed by different weight of water droplet from varying its volume, the  $F_{ex}$  could be also equally affected by the difference of the surface areas and  $d_{\text{droplet}}$  of the water droplets as shown in eqn (2) and (4). Therefore, as shown in Fig. 3b, the experimental- $F_{ex}$  of 3  $\mu\text{L}$  and 7  $\mu\text{L}$  water droplets was similar to the corresponding simulated- $F_{ex}$ . These results indicated that our electrostatic-induced trajectory switching system can be operated in the same tilt angle condition despite the different volumes of the water droplets. Furthermore, we believe that the sub-microliter droplet can also be controlled in our system due to the almost-zero adhesion force between droplet and superhydrophobic guiding track.

To observe the critical conditions of the electrostatic-induced trajectory switching system, further experiments were conducted by altering the substrate-tilt angle and the applied voltage. For each condition, 5  $\mu\text{L}$  water droplets were dropped on the PFDT Ag/Cu guiding track and a 1 kV DC bias was applied to one of the patterned capacitors. While operating the

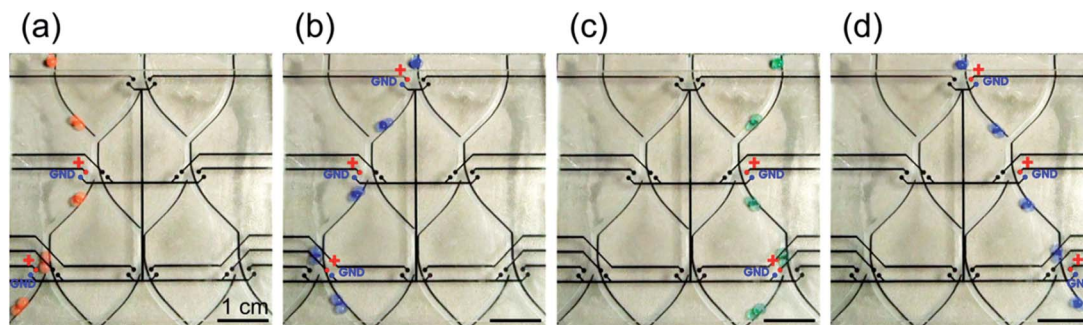


Fig. 4 Sequential photographic images of a 5  $\mu\text{L}$  water droplet on the three inlet, four outlet PFDT Ag/Cu guiding track located under a circuit-patterned glass slide when the capacitors of the patterned circuit were selectively applied with a 1 kV DC bias to guide the water droplet along the intended trajectory: (a) from inlet 1 to outlet 1, (b) from inlet 2 to outlet 2, (c) from inlet 3 to outlet 3, and (d) from inlet 2 to outlet 4 (see the Video S2†).

electrostatic-induced trajectory switching system, there are three possible results: ‘misguided’, ‘guided’, and ‘trapped’. ‘Misguided’ is defined as the scenario where the water droplet deviates from the intended trajectory of the PFDT Ag/Cu guiding track. Similarly, ‘guided’ is defined as when the water droplet is successfully guided on the intended trajectory. Finally, ‘trapped’ is defined as the situation where the water droplet stops at the junction of the PFDT Ag/Cu guiding track. We have included the summary of these three phenomena in Fig. 3c, which represents the experimental results as a function of substrate-tilt angle and the applied voltage. In the red region, the experiments were performed with a high substrate-tilt angle and low applied voltage (ratio of  $F_g$  and  $F_{ex}$ ,  $F_g/F_{ex} > 2.93$ ). In this case, since the water droplet was mainly dominated by the  $F_g$ , the water droplet was misguided. The large  $F_g$  could be described same as large inertial force. If the  $F_g$  is larger than  $F_{ex}$ , the droplet is not controllable because the inertial force which is the tendency to roll off the water droplet along the guiding track regardless of the direction, would be dominant. On the other hand, in the blue region,  $F_{ex}$  was stronger than  $F_g$  due to the low substrate-tilt angle and the high applied voltage ( $F_g/F_{ex} < 1.04$ ). Because the water droplet was mainly governed by the  $F_{ex}$ , the water droplet was trapped on the PFDT Ag/Cu guiding track. As shown in the green region, when  $F_g$  and  $F_{ex}$  were balanced ( $1.04 \leq F_g/F_{ex} \leq 2.93$ ), the water droplet was successfully guided along the intended trajectory of the PFDT Ag/Cu guiding track. Furthermore, to stably operate the electrostatic-induced trajectory switching system, the  $\theta_{SA}$  and the applied voltage should be maintained below  $15^\circ$  and 1.4 kV, respectively.

As a proof of concept, we applied an electrostatic-induced trajectory switching system to MIMO open channel microfluidics, as shown in Fig. 4a–d and the Video S2.† In this experiment, the PFDT Ag/Cu guiding track was designed with three inlets and four outlets and located under a circuit-patterned glass slide containing 12 capacitors. The guiding track and capacitor-patterned glass slide were aligned in parallel, with a distance of 2 mm between them and tilted with a low tilt angle of  $5^\circ$ . Fig. 4a–d show the time-sequential optical images of 5  $\mu\text{L}$  water droplets moving on the PFDT Ag/Cu guiding track under a 1 kV DC bias selectively applied to the capacitors of the patterned circuit. Moving droplets were dyed orange, blue, and green at inlet 1, 2,

and 3, respectively. DC-biased capacitors are emphasized and colored red at the anodes and blue at the cathodes. As shown in Fig. 4a, the orange-dyed water droplet from inlet 1 was guided to outlet 1 along the selected trajectory. The green-dyed water droplet from inlet 3 was also successfully guided to outlet 3 in Fig. 4c. Similarly, the blue-dyed water droplets from inlet 2 were guided to outlets 2 or 4, as intended, in Fig. 4b and d. We could easily control the trajectory of a moving water droplet by selectively applying DC bias on capacitors in a MIMO open channel microfluidic system.

## Conclusions

In summary, we demonstrated a facile method to fabricate a MIMO open channel microfluidic system that can switch the trajectory of a moving water droplet on a superhydrophobic guiding track using electrostatic force. The superhydrophobic droplet guiding track was obtained by growing Ag nanostructures on the track-sculptured Cu plate and coating PFDT on the Ag/Cu guiding track. Water droplets were easily rolled-off along the PFDT Ag/Cu guiding track, and the trajectory of droplets could be switched by selectively applying a DC bias to capacitors patterned on the glass slide located above the substrate. When charges were accumulated at the DC-biased capacitor, the electrostatic force was exerted on the surface of water droplet and attracted the droplet toward the capacitor at the junction of the PFDT Ag/Cu guiding track. The electrostatic-induced trajectory switching system can only successfully operate when the electrostatic force was appropriately balanced with the gravitational force of the water droplet. This electrostatic-induced trajectory switching system was applied to a MIMO superhydrophobic droplet guiding track with three inlets and four outlets. We expect that this high-speed, contamination-free, and facile droplet guiding technology has great potential to be utilized in advanced functional open-channel lab-on-a-chip applications such as *in situ* biomolecule detectors and micro reactors.

## Note added after first publication

This article replaces the version published on 19th December 2014, in which the corresponding author was missing.

## Acknowledgements

This work was supported by the Priority Research Centers Program through the National Research Foundation of Korea (NRF) funded by the Ministry of Education, Science and Technology (MEST) (2012-0006689) and by Mid-career Researcher Program through NRF grant funded by the MEST (2014R1A2A2A09053061). This work was also supported by the Industrial strategic technology development program (10041041, development of nonvacuum and nonlithography based 5  $\mu\text{m}$  width Cu interconnect technology for TFT backplane) funded by the Ministry of Knowledge Economy (MKE, Korea). In addition, the authors would like to acknowledge the support of the Ministry of Higher Education, Kingdom of Saudi Arabia for supporting this research through a grant (PCSED-009-14) under the Promising Centre for Sensors and Electronic Devices (PCSED) at Najran University, Kingdom of Saudi Arabia. We thank the Tanaka Kikinzoku Kogyo K. K. for comments on the usage of silver.

## Notes and references

- 1 M. Washizu, *IEEE Trans. Ind. Appl.*, 1998, **34**, 732–737.
- 2 A. C. Hatch, J. S. Fisher, S. L. Pentoney, D. L. Yang and A. P. Lee, *Lab Chip*, 2011, **11**, 2509–2517.
- 3 I. You, S. M. Kang, S. Lee, Y. O. Cho, J. B. Kim, S. B. Lee, Y. S. Nam and H. Lee, *Angew. Chem., Int. Ed.*, 2012, **51**, 6126–6130.
- 4 W. Dungchai, O. Chailapakul and C. S. Henry, *Anal. Chem.*, 2009, **81**, 5821–5826.
- 5 D. Belder, *Angew. Chem., Int. Ed.*, 2005, **44**, 3521–3522.
- 6 A. R. Parker and C. R. Lawrence, *Nature*, 2001, **414**, 33–34.
- 7 S. K. Cho, H. Moon and K. Chang-Jin, *J. Microelectromech. Syst.*, 2003, **12**, 70–80.
- 8 J. Seo, S. Lee, J. Lee and T. Lee, *ACS Appl. Mater. Interfaces*, 2011, **3**, 4722–4729.
- 9 H. Mertaniemi, V. Jokinen, L. Sainiemi, S. Franssila, A. Marmur, O. Ikkala and R. H. Ras, *Adv. Mater.*, 2011, **23**, 2911–2914.
- 10 H. Gau, S. Herminghaus, P. Lenz and R. Lipowsky, *Science*, 1999, **283**, 46–49.
- 11 L. Hong and T. Pan, *Microfluid. Nanofluid.*, 2011, **10**, 991–997.
- 12 Z. Nie, C. A. Nijhuis, J. Gong, X. Chen, A. Kumachev, A. W. Martinez, M. Narovlyansky and G. M. Whitesides, *Lab Chip*, 2010, **10**, 477–483.
- 13 M. Elsharkawy, T. M. Schutzius and C. M. Megaridis, *Lab Chip*, 2014, **14**, 1168–1175.
- 14 X. Zhang, M. Jin, Z. Liu, S. Nishimoto, H. Saito, T. Murakami and A. Fujishima, *Langmuir*, 2006, **22**, 9477–9479.
- 15 H. Zhou and S. Yao, *Lab Chip*, 2013, **13**, 962–969.
- 16 M. Gunji and M. Washizu, *J. Phys. D: Appl. Phys.*, 2005, **38**, 2417.
- 17 D. t. Mannetje, S. Ghosh, R. Lagrauw, S. Otten, A. Pit, C. Berendsen, J. Zeegers, D. van den Ende and F. Mugele, *Nat. Commun.*, 2014, **5**, 3559.
- 18 Y. Zhang and T. H. Wang, *Adv. Mater.*, 2013, **25**, 2903–2908.
- 19 L. W. Wang, C. Yang and C. M. Li, *Lab Chip*, 2009, **9**, 1504–1506.
- 20 L. H. Hung, K. M. Choi, W. Y. Tseng, Y. C. Tan, K. J. Shea and A. P. Lee, *Lab Chip*, 2006, **6**, 174–178.
- 21 X. Niu, S. Gulati, J. B. Edel and A. J. deMello, *Lab Chip*, 2008, **8**, 1837–1841.
- 22 D. R. Link, S. L. Anna, D. A. Weitz and H. A. Stone, *Phys. Rev. Lett.*, 2004, **92**, 054503.
- 23 H. Kawamoto, *J. Electrostat.*, 2009, **67**, 850–863.
- 24 I. A. Larmour, S. E. Bell and G. C. Saunders, *Angew. Chem., Int. Ed.*, 2007, **46**, 1710–1712.
- 25 N. A. Patankar, *Langmuir*, 2004, **20**, 8209–8213.
- 26 S. Y. Park, S. Kalim, C. Callahan, M. A. Teitell and E. P. Chiou, *Lab Chip*, 2009, **9**, 3228–3235.
- 27 J. Seo, S. Lee, H. Han, H. B. Jung, J. Hong, G. Song, S. M. Cho, C. Park, W. Lee and T. Lee, *Adv. Mater.*, 2013, **25**, 4139–4144.
- 28 J. Seo, J. S. Lee, K. Lee, D. Kim, K. Yang, S. Shin, C. Mahata, H. B. Jung, W. Lee, S. W. Cho and T. Lee, *Adv. Mater.*, 2014, **26**, 7043–7050.